IPHC - CNRS - Université de Strasbourg

A MAPS digitiser
Building a digitiser algorithm for CMOS/MAPS sensors with analog or digital output

Author: Auguste BESSON (abesson in2p3.fr)
Date: March 4^{th} 2012

Abstract

We present an overview of an algorithm which simulates the response of a CMOS/MAPS pixel sensor (CPS) which can be implemented in a complete simulation program. It includes the simulation of the charge deposition, the charge transport in the the digital response (ADC or discriminator) of the sensor. The algorithm is based on a data driven approach and uses extensively the result of test beam data performed by the IPHC group (and collaborators) on various sensors, both with analog or digital output. The algorithm gives as an output a list of pixels hit with their corresponding signal. It is able to take into account the incident angle of the impinging charged particle which crosses the detector. Results and performances of the algorithm are compared with test beam data. It is shown that the multiplicity of the clusters, the resolution and the efficiency of the sensor are correctly reproduced with a precision of the order of 10 %.

1 Introduction

CMOS Pixel Sensors (CPS)[1], have been developed during the last twelve years for the advent of a new generation of vertex detectors, where priority is given to granularity, material budget and power consumption, potentially at the expense of read-out speed and radiation tolerance. Being initially developed for an experiment at the ILC, the sensors came out to be well suited to Heavy Ion Collision experiments, and their intrinsic potential offers attractive perspectives for the vertex detector to be operated at the SuperB factory. They have reached a level of maturity allowing them to equip successfully beam telescops (EUDET project) and for the first time, a complete vertex detector (STAR-HFT) equipped with this type of sensors. Furthermore, CPS are also foreseen in other project (large area beam telescope for the EU-FP7 project AIDA) or are considered as option (CBM experiment vertex detector, ALICE ITS Upgrade, superB, etc.).

Analog processing of the signal (preamplification, pedestal subtraction) takes place in the pixel itself. For the sake of granularity and power consumption, the mixed and digital signal processing micro-circuits complementing the signal processing (charge encoding, sparsification, etc.) are integrated on the sensor substrate at the chip periphery. The chip read-out is then based on a rolling shutter architecture where the pixels are organised in columns read out in parallel. This share of functionnalities is a basic feature of the MIMOSA sensors developed by the IPHC-IRFU collaboration [2].

One of the particularities of CPS is that the sensitive volume, i.e. the epitaxial layer remains mostly undepleted. The electrons, coming from the ionising charged particles crossing the detector, diffuses thermaly in the epi. layer and are finally collected by N-well diodes. Charge sharing between pixels is then enhanced leading to cluster of typically 3 to 9 pixels with a Signal-to-Noise ratio above $\simeq 5$. Additonnal effects occur like recombination, reflexion of the electrons at the epi-substrate interface. These effects depend mostly on not so well known parameters like the doping profile, the epitaxial layer thickness, etc. This forced us to chose a pragmatical approach and to build a data driven model based on the available information one can get in laboratory tests and beam tests. The typical measurable information are the collected charge (for chips with analog output), charge distribution between pixels, Noise, charge collection efficiency, ADC gain and dynamic range. Hopefully, during the last ten years, the PICSEL group of IPHC (and collaborators) realized more than 30 test beam campaigns (mostly at DESY and CERN) on many different prototypes, and one can take advantage of this unique and huge amount of information.

The final goal is to be able to simulate the charge deposition, the charge transport and collection and finally the digitisation. Since these processes are not directly measurable, the global performances of the algorithm will then be compared on different cross-check distributions based on different set of data. These test distributions will be mainly the cluster multiplicity (driving the occupancy), the efficiency, the resolution, and hit separation power. Since the fake rate depends on many other features, it will not be considered as a test criteria.

The first section presents the algorithm and the approach to simulate the charge transport up to the pixels. Then the performances of the model are compared with different test beam data with different prototpyes, pixel pitches, with analog our digitised output. Finally the incident angle effect is studied.

2 General strategy

In the present note, one will consider that the incident particle is a Minimum Ionizing Particle (M.I.P.). The algorithm should be able to reproduce the response of a given CPS for any incident M.I.P. at any angle. To perform simulation in particle

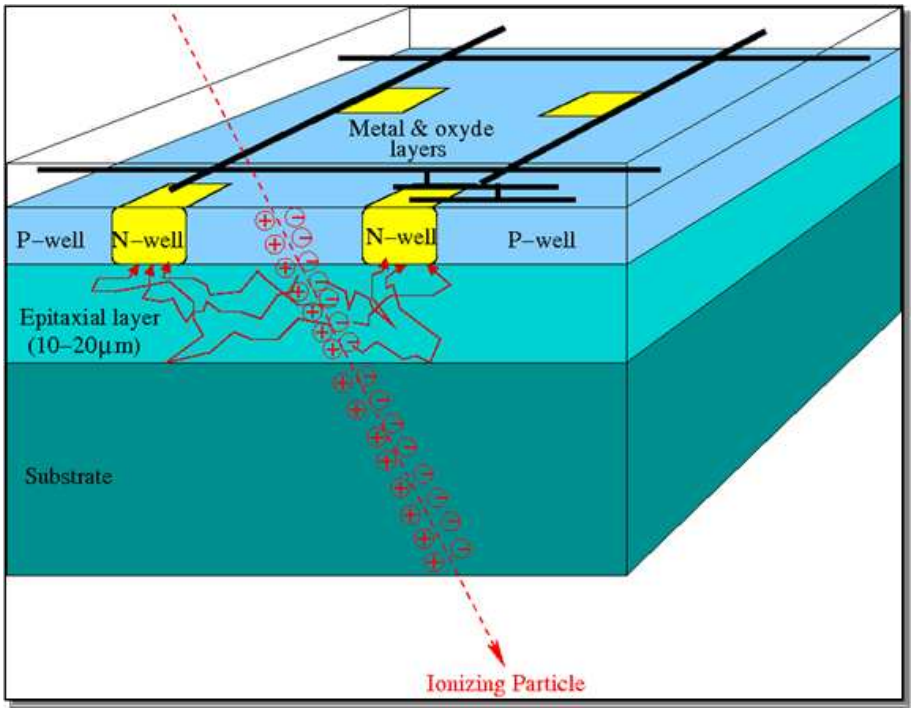

Figure 1: 3D Scheme of a CMOS pixel sensor.

physics experiment, one generally uses GEANT-4 which provides entry and exit points of a given detector volume. The present algorithm needs only this information as an input from the considered experiment simulation. In addition, a different set of parameters obtained from test beam data are used to simulate the following steps:

- Energy deposition and electron-hole pair creation along the path in the epitaxial layer.
- Charge transport up to the N-well charge collecting diodes through thermal diffusion.
- Digital conversion of the collected charge (Discriminator, ADC, zero suppression).

The following subsections describe these three steps.

2.1 Energy deposition

The energy deposition depends on the path of the incident particle trough the epitaxial layer. If epi is the epitaxial layer thickness and if θ is the angle between the incident particle path and the direction perpendicular to the sensor plane, the effective thickness t is just $epi/\cos\theta$. The energy deposition is directly translated into a number of electron/hole pair creation ($3.6\ eV/e^-$). In the following discussion, one will consider the frame (x, y, z) with x and y in the sensor plane and z perpendicular to the sensor plane.

The driving parameters allowing to generate the energy deposition are:

- The distribution of a Landau law, with a MPV value of $80\ e^-/\mu m$.
- The width of the Landau law depends on the total effective thickness. Based on experimental test beam data, a value of $18\ e^-/\mu m$ has been chosen.
- An effective epitaxial thickness used as an adjustable parameter.

One should note that the effective epitaxial thickness is not necessarly close to a measured one since it includes secondary effects like electrons recombination and charge collection inefficiencies, electron creation within the collecting diode, possible slope in the doping profile, reflexion of the charge at the epi/substrate interface, etc. This parameter depends highly on the considered prototype (process technology, resistivity, pitch, didoe sizes, etc.), and has to be adjuted with experimental data. So, since the charge recombination do exists, the charge collection efficiency is not 100 %. In practice it has been measured routinely in the range of 85 % to 95 %, on a lot (~ 30) of different chips during the last decade.

2.2 Charge transport

The created electrons along the track thermally diffuse in the epitaxial layer because the depleted volume tends to be small around the collecting diodes (generally few microns in depth depending on the resistivity). Most of the electrons are then collected by several N-well diodes leading to a cluster of hit pixels. Thus, the charge sharing between pixels is enhanced with respect to classical depleted detectors. By computing a simple center of gravity of the charges or by using more sophisticated algorithms (like the so-called η functions), the charge sharing allows to obtain a significantly better resolution than the simple digital resolution ($\sigma_{digital} = pitch/\sqrt{12}$. This statement remains true with digital output sensors (see figure 13).

Another hypothesis is assumed concerning the distribution of the charge along the path. In the present algorithm, the charge is equally distributed along the path crossing the epitaxial layer. This path is divided in N segments. with a deposited charge equal to $(total\ \ charge)/N$ in the middle of each segment. N can be chosen in such a way that there is only one electron per segment leading to a maximized precision but a larger computing time. The main purpose of this approach is to be able to reproduce the charge deposition of any incident particle with any incident angle. One should note that the depth position of the segment (i.e. the z coordinate) is not taken into account in the algorithm. Only the x and y position are used. Building an algorithm using the z position of the segments could be possible to the price of additionnal free parameters to be adjusted.

One can summarize the procedure:

- each track has an entry point and an exit point in the epitaxial layer.
- The tracks is divided in N segments of equal sizes. Total created charge Q_{tot} is shared equally between the N segments. $Q_i = Q_{tot}/N$ can be as low as $1\ e^-$.
- Depending on the x and y position of the segment and on the position of the 25 diodes around, the 25 probabilities that the charge Q_i is collected by the diode j ($j = 1, 25$) are computed thank to the probability density function (see next section). Then a random number is generated and the charge Q_i is deposited in one of the 25 diodes.
- The procedure is repeated for the N segments and the total collected charge on each diode is computed.

2.3 Digitisation

At this stage, the analog collected charge on each diode is known. The pixel noise (in electrons units) is then added on each pixel, depending on the measured noise of the considered prototype. This noise is actually not gaussian and an approximation is made here.

The following steps consists in simulating the digitisation process, depending on the considered prototype. Some of the prototypes deliver an analog output (actually, the charge is usually encoded on 12 bits), whereas others delivers a pure digital output or delivers an output encoded with a 2 to 5 bits ADC. Furthermore, a zero suppression stage can exist. An ideal reponse of the ADC/discriminator is assumed, so only the dynamic range and the Least Significant Bit (or the discriminator thrshold) is used as an input.

The ADC/digitisation response of the sensor should be smeared due to the temporal noise and fixed patern noise in the digitisation process. One additionnal steps could be added consisting in adding noisy pixels to reproduce correctly the correct fake hit rate obtained with data. These last two steps are not included in the present study, but could be added easily.

2.4 DIGMAPS tool

To compare the different algorithm perfomances with the data, and to optimize the set of parameters which reproduces the most corrrectly the data, a standalone tool have been developped. This software tool, named *DIGMAPS*, run with ROOT [**?**] and is able to simulate the response of a CPS with various options (incident angle of the ongoing particles, pitch, epitaxial layer, ADC/discri thresholds, etc. The software tool is public and available on demand [3]. All the results of the following sections have been obtained with this tool.

3 Building the probability density function

The probability density function is the core of the algorithm and depends higlhy on the CPS sensor. As it has been discussed previously, The physical parameters influencing the charge transport are too numerous and in general not measured with a satisfactory precision to allow to build a theoritical model reproducing the probability density function (PDF). Thus, a pragmatical approach has been prefered. The first attempt to build the PDF has been performed based on a set of chips in the AMS $0.35\ \mu m$ opto technology because different CPS prototypes with various pitches (from 10 to $40\ \mu m$) and with analog output had been fabricated and fully characterized in laboratory and in test beam facilities. The PDF distributions

Chip							
	M18	M9	M9	M9	M9	M9	M9
Pitch (μm)							
	10	20	20	30	30	40	40
Diode size (μm^2)							
	3.4×4.3	3.4×4.3	6×6	3.4×4.3	5×5	3.4×4.3	6×6
Charge (MPV) in the seed pixel (electrons)							
	313.5 $\pm$ 0.5	250.4 $\pm$ 0.3	338.8 $\pm$ 0.4	203.6 $\pm$ 0.7	248.2 $\pm$ 1.2	181.4 $\pm$ 0.2	251.4 $\pm$ 0.3
Total Charge (MPV) in the 9 highest charge collected pixels (electrons)							
	906.4 $\pm$ 1.6	765.1 $\pm$ 1.1	897.4 $\pm$ 0.9	625.3 $\pm$ 2.3	716.0 $\pm$ 3.7	568.1 $\pm$ 0.5	717.1 $\pm$ 0.7
Total Charge (MPV) in a 5×5 cluster (electrons)							
	1011.8 $\pm$ 2.0	863.3 $\pm$ 1.4	938.7 $\pm$ 1.0	695.1 $\pm$ 2.9	776.5 $\pm$ 4.8	622.4 $\pm$ 0.7	742.5 $\pm$ 0.9
Average noise (electrons)							
RMS	10.9 $\pm$ 0.8	9.2 $\pm$ 1.1	12.3 $\pm$ 1.4	9.5 $\pm$ 1.1	11.4 $\pm$ 1.2	9.8 $\pm$ 1.3	13.0 $\pm$ 1.6
$RMS/\sqrt{N}$	$\pm$ 0.02	$\pm$ 0.02	$\pm$ 0.02	$\pm$ 0.03	$\pm$ 0.03	$\pm$ 0.02	$\pm$ 0.03
Signal to Noise ratio (MPV) in the seed pixel							
	28.0 $\pm$ 0.4	26.3 $\pm$ 0.3	26.8 $\pm$ 0.3	21.1 $\pm$ 0.3	22.1 $\pm$ 0.4	18.4 $\pm$ 0.2	19.4 $\pm$ 0.2

Table 1: Measured collected charges, Noise and S/N for Mimosa9-18 sensors.

were obtained with data and several functions were tried to fit the data with a reasonnable amount of parameters. A relatively simple and satisfactory function was the sum of a gaussian and a lorentzian.

4 Analog output: Mimosa 9/18 results

5 Digital output with high resistivity epitaxial layer: Mimosa 28 (a.k.a. Ultimate) results

For many years, CPS were manufactured with commercial wafers featuring exclusively low resistivity (i.e. typically $10\ \Omega{\cdot}cm$) epitaxial layers. The interest of industry for high resistivity epitaxial layers is a rather recent event, with a considerable impact on the potential of the CPS (e.g. a typical signal-to-noise ratio of about 35-40). The main consequence of the high resistivity is to enhance the depleted region around the collecting diodes. Charge transport is then complexified since undepleted regions (far from the diodes) and depleted regions (close to the diodes) coexists. The basic data driven model has to be modified to take into account this effect leading to a "screening effect" and thus modifying the probability density functions.

Several sensors were fabricated since early 2010 with a $> 400\ \Omega \cdot cm$ resistivity epitaxial layer, available in a $0.35\ \mu m$ process, and tested on particle beams. The Mimosa-28 prototype, also named Ultimate sensor has been built in this process and will equip the STAR-HFT.

The first vertex detector equipped with CPS is currently being built for the STAR experiment at RHIC. Named STAR-PXL, it is composed of two cylindrical layers, with radii of 2.5 and 8 cm (see figure **??**). It is built from 40 ladders, each made of 10 sensors and featuring a total material budget of $0.37\%\ X_0$ per layer. The 400 sensors equipping the detector correspond to $\simeq 370$ Mpixels.

The ULTIMATE sensor, designed in the AMS-$0.35\ \mu m$-OPTO technology, comprises 928×960 pixels with $20.7\ \mu m$ pitch and a $15\ \mu m$ thick, high resistivity ($> 400\ \Omega \cdot cm$) epitaxial layer, and includes radiation tolerant structures. Its power consumption amounts to $\lesssim 135\ mW/cm^2$, corresponding to $\sim 0.8\ \mu W$ per pixel. The read-out time following from the rolling shutter architecture is $< 200\ \mu s$. The sensor delivers a binary signal based on discriminators ending each of the 928 columns followed by a zero suppression micro-circuitry. It is suited to a flux of 10^6particles$/cm^2/s$.

The sensor has been tested with a 120 GeV/c pion beam at the CERN-SPS in July 2011, in running conditions approaching those of the STAR-PXL (e.g. T= 30^oC, $150\ kRad$ ionising dose). The chip reaches a detection efficiency $\gtrsim 99.9\%$ even

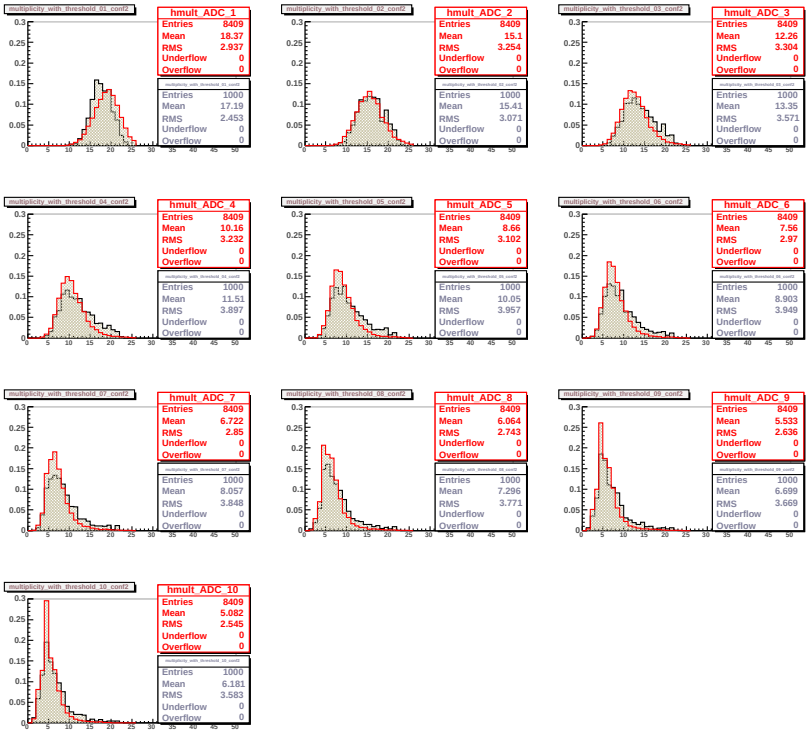

Figure 2: cluster multiplicity distribution for various ADC cuts (from top left to top right, Signal $\geq$ 1,2,3,4,5,6,7,8,9,10 ADC units).
For Mimosa 18, analog output, pitch $= 10\mu m$, 1 ADC unit $= 7.0\ e^-$, Noise $= 10.9\ e^-$.

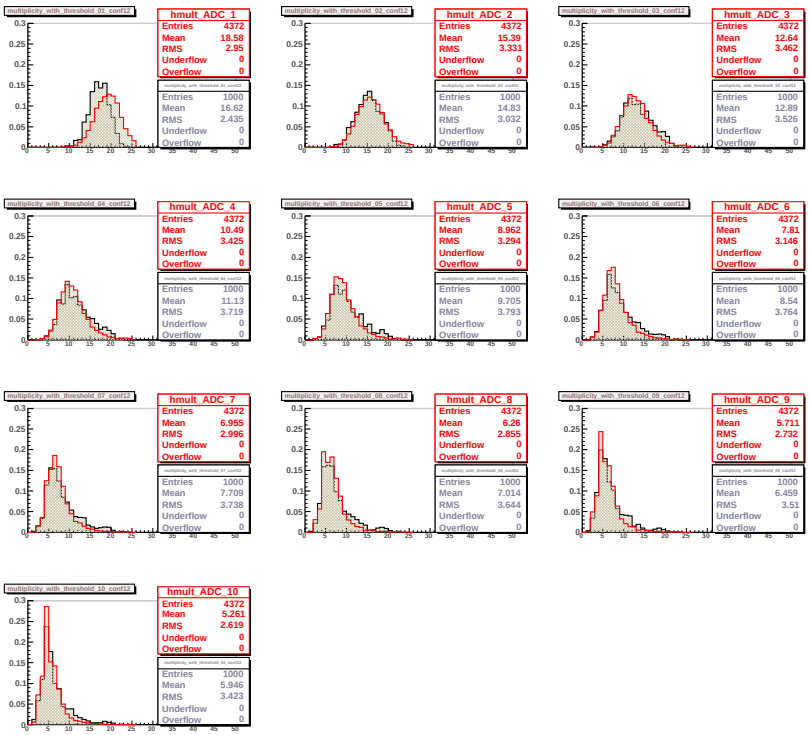

Figure 3: cluster multiplicity distribution for various ADC cuts (from top left to top right, Signal $\geq$ 1,2,3,4,5,6,7,8,9,10 ADC units).
For Mimosa 9, analog output, pitch $= 20\mu m$, 1 ADC unit $= 5.9\ e^-$, Noise $= 9.2\ e^-$.

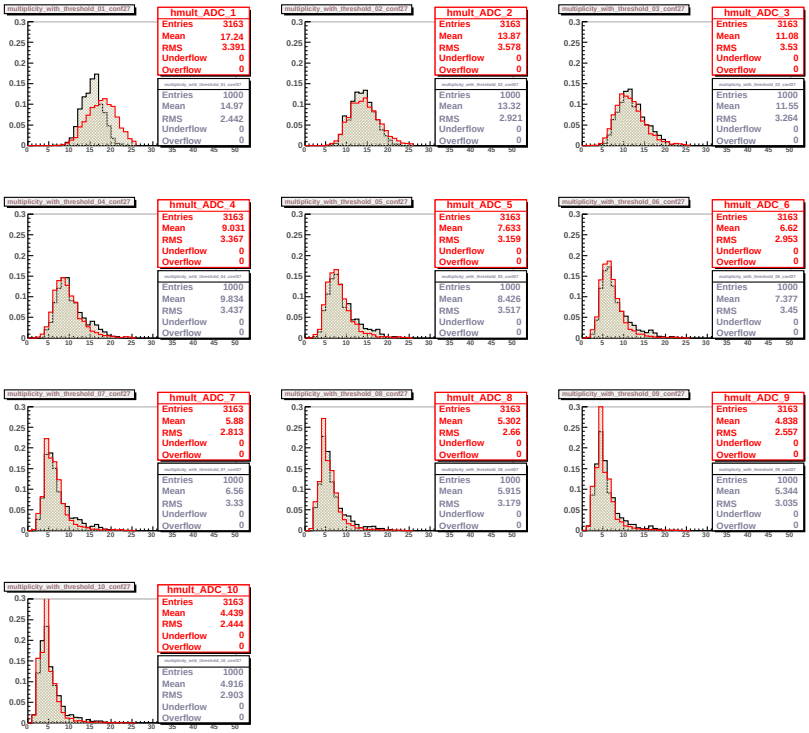

Figure 4: cluster multiplicity distribution for various ADC cuts (from top left to top right, Signal $\geq$ 1,2,3,4,5,6,7,8,9,10 ADC units).
For Mimosa 9, analog output, pitch $= 30\mu m$, 1 ADC unit $= 5.9\ e^-$, Noise $= 9.4\ e^-$.

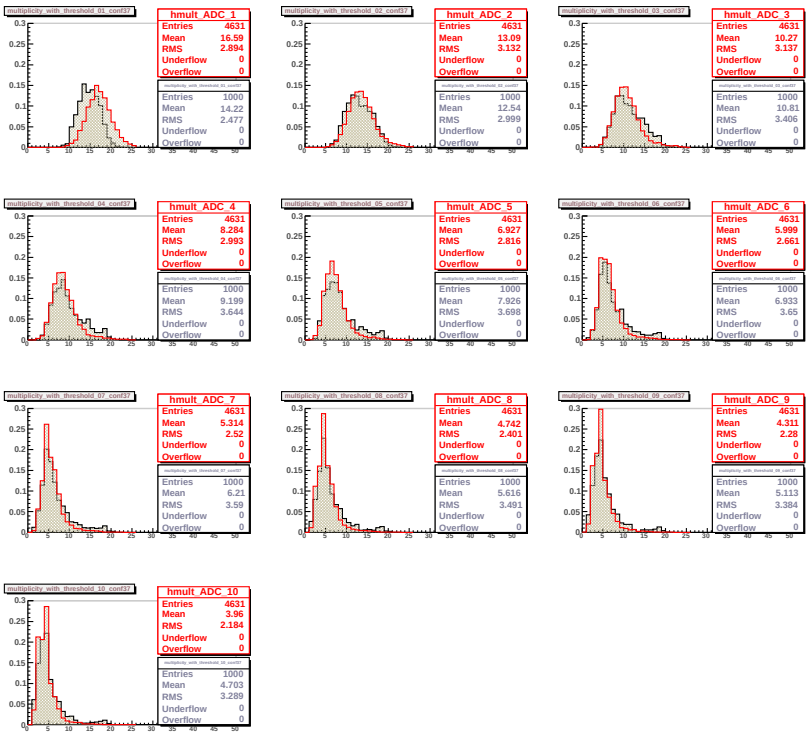

Figure 5: cluster multiplicity distribution for various ADC cuts (from top left to top right, Signal $\geq$ 1,2,3,4,5,6,7,8,9,10 ADC units).
For Mimosa 9, analog output, pitch $= 40\mu m$, 1 ADC unit $= 5.9\ e^-$, Noise $= 9.8\ e^-$.

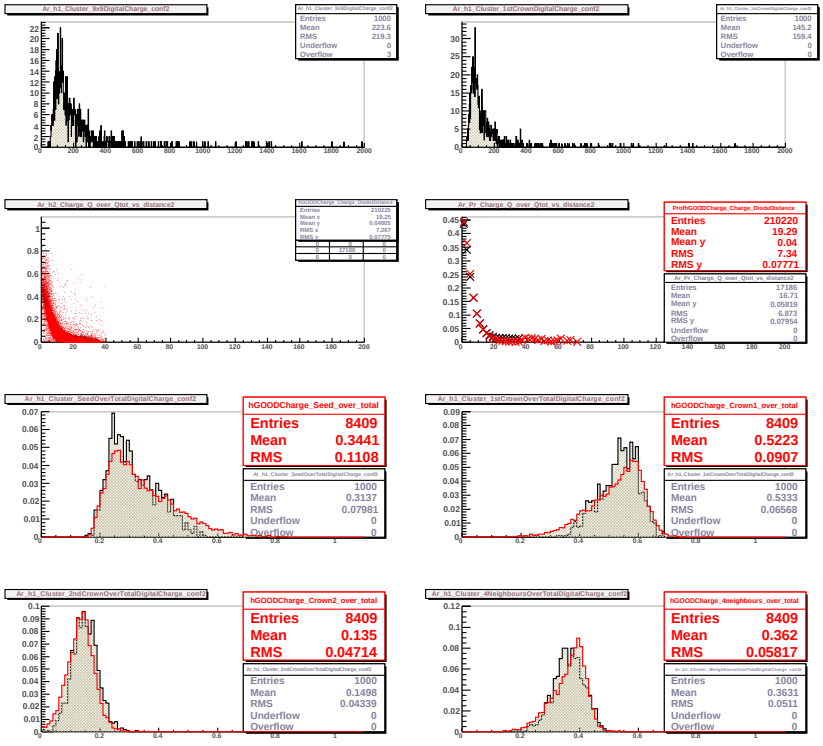

Figure 6: cluster multiplicity distribution for various ADC cuts (from top left to top right, Signal $\geq$ 1,2,3,4,5,6,7,8,9,10 ADC units).
For Mimosa 18, analog output, pitch $= 10\mu m$, 1 ADC unit $= 7.0\ e^-$, Noise $= 10.9\ e^-$.

for high discriminator threshold values, where the fake hit rate (due to pixel noise fluctuations) is below 10^{-6}. Providing moreover a spatial resolution of $\simeq 3.7\ \mu m$, the sensor is proven to meet the most important STAR-PXL requirements.

5.1 Probability density function

The probability density function is obtained from data.

$$p(d) \quad = \quad N_0 \times e^{\frac{-(d-d_0)^2}{2\sigma^2}} + N_1 \times \frac{\Gamma}{(d-d_1)^2 + \Gamma^2} \tag{1}$$

where:

- d = distance between the segment position and the center of the considered diode
- N_0, d_0, N_1 Γ and d_1 are fit parameters

6 Resolution studies and comparisons

7 Angular studies for Ultimate sensor

An important cross-check needs to be made to test if the model behaves correctly when the incident particle has a non-zero angle with respect to the perpendicular direction of the plane. One can notes that the model has not been tuned to take into account possible distorsion of the cluster multiplicity when the angle increases. However, since the charge transport is

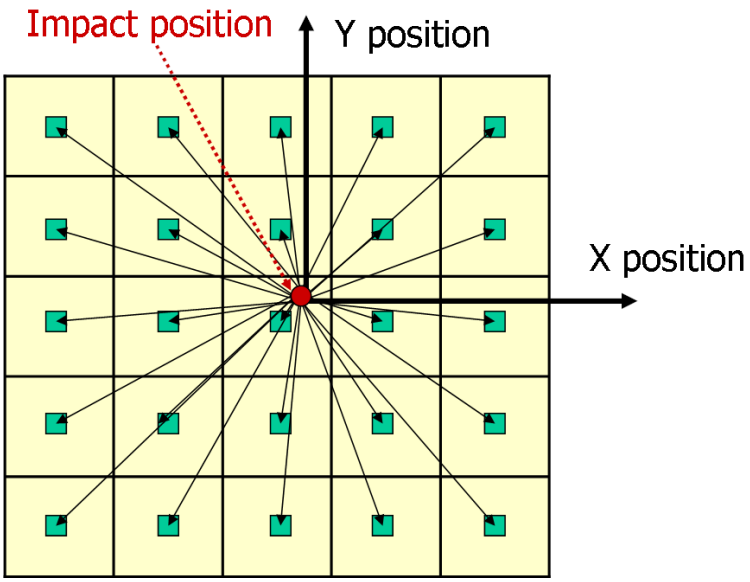

Figure 7: Definition of the 25 distances between impact position and the 25 diode positions.

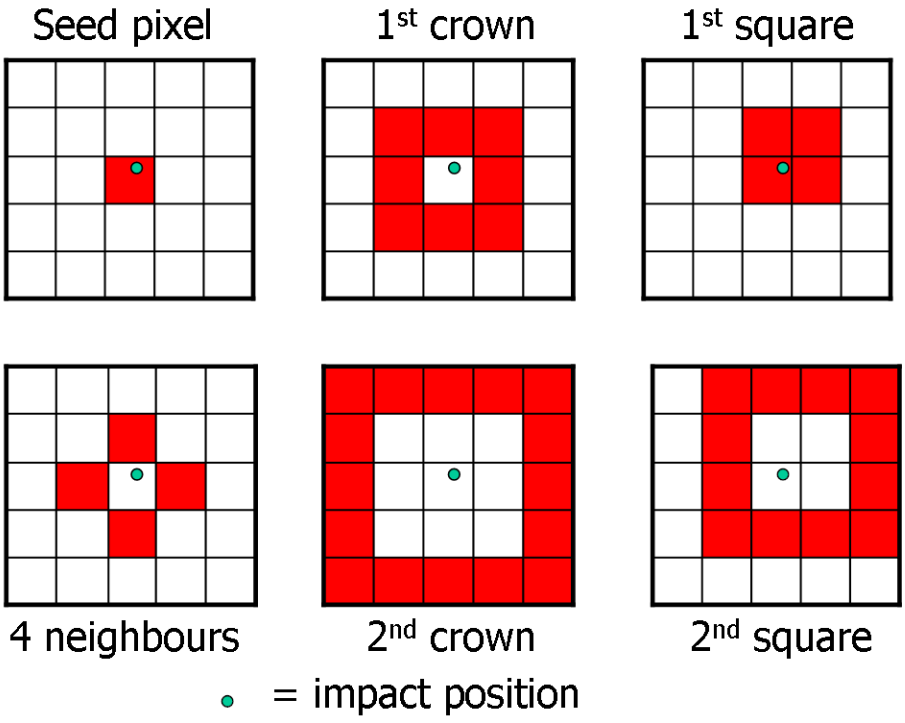

Figure 8: Definition of the so called, seed pixel, 4 neighbour pixels, first and second crown, first and second square with respect to the impact position.

First square pixels					
N_0	d_0	σ	Γ	d_1	N_1
0.458	-3.98	13.2	3.99	1.80	6.45
Other pixels					
N_0	d_0	σ	Γ	d_1	N_1
0.117	-1.07	17.5	47.1	-4.64	3.71

Table 2: Fit parameters of the probability density function obtained from Ultimate sensor test beam data.

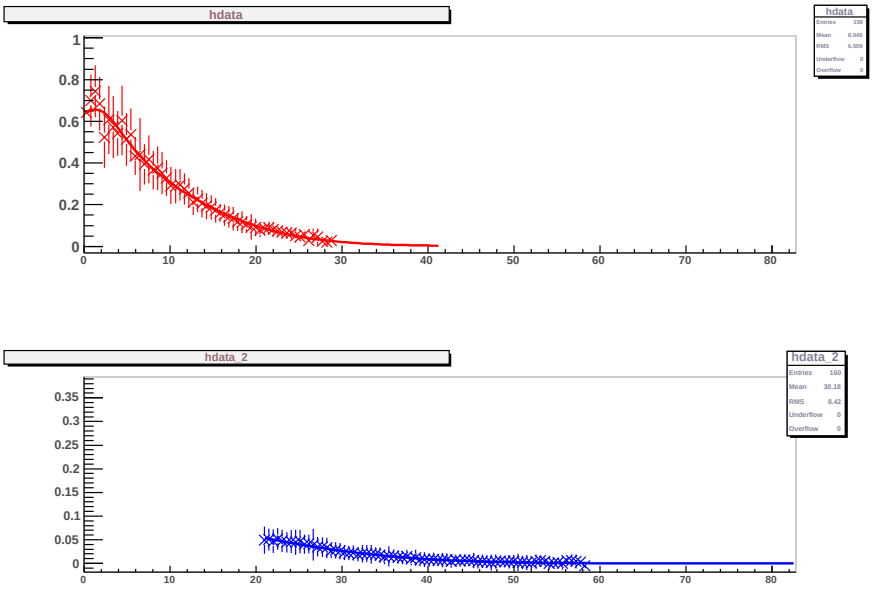

Figure 9: Probability density function for the first (top, red) and the second (bottom, blue) square of pixels around the hit position versus the diode-hit distance

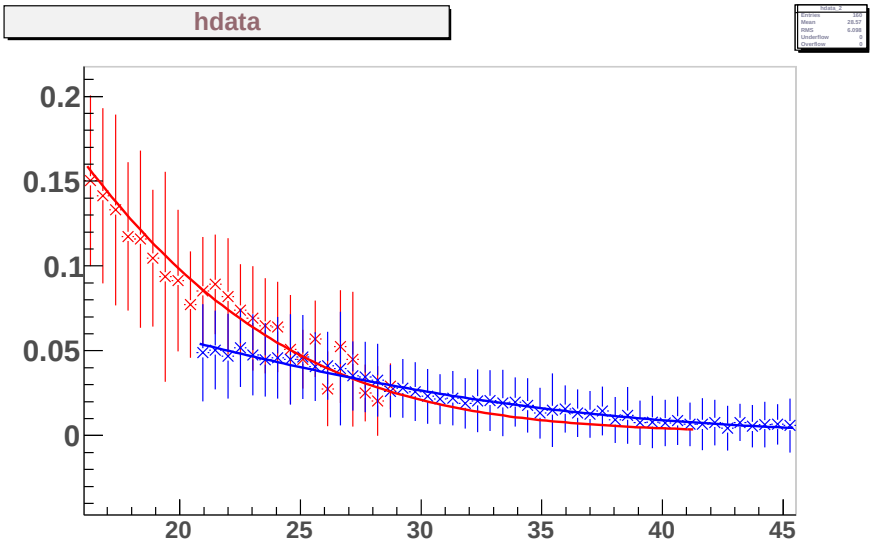

Figure 10: Probability density function for the first (red) and the second (blue) square of pixels around the hit position versus the diode-hit distance zoomed in the range $[pitch; pitch \times \sqrt{2}]$.

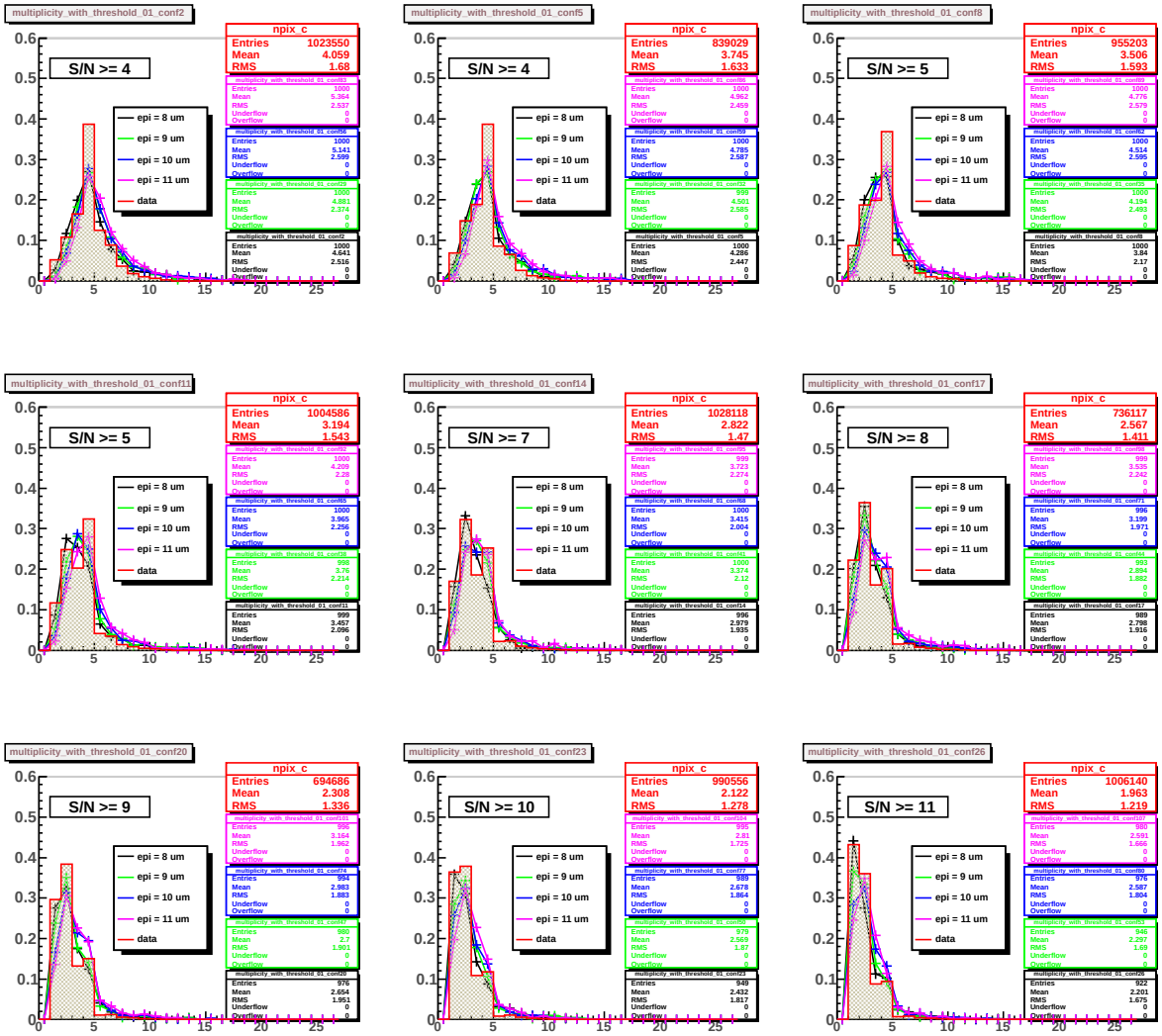

Figure 11: Cluster Multiplicity distribution for 9 different discriminator thresholds (from up left to bottom right, S/N $\geq$ 4.0, 4.5, 5.0, 5.8, 7.0, 8.0, 9.0, 10.2, 11.5).
a. red line filled in brown represents ultimate test beam data.
b. The four other colors represent the digitiser model with 4 different effective epitaxial layer thickness: black = 8 μm, green = 9 μm, blue = 10 μm, pink = 11 μm.

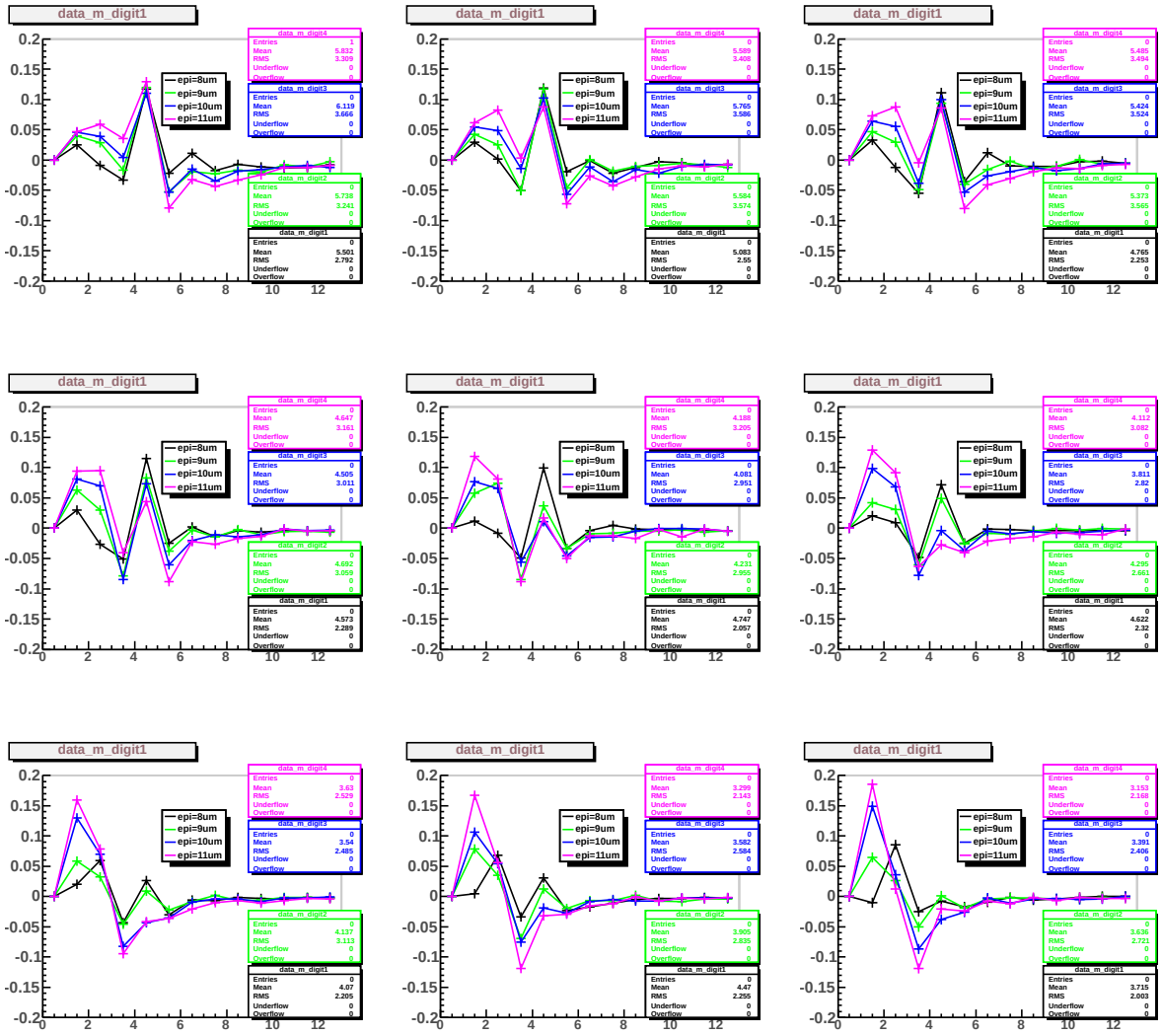

Figure 12: For 9 different discriminator thresholds (from up left to bottom right, S/N $\geq$ 4.0, 4.5, 5.0, 5.8, 7.0, 8.0, 9.0, 10.2, 11.5), cluster multiplicity bin by bin difference between data and simulation models with 4 different effective epitaxial layer thickness: black = 8 μm, green = 9 μm, blue = 10 μm, pink = 11 μm.

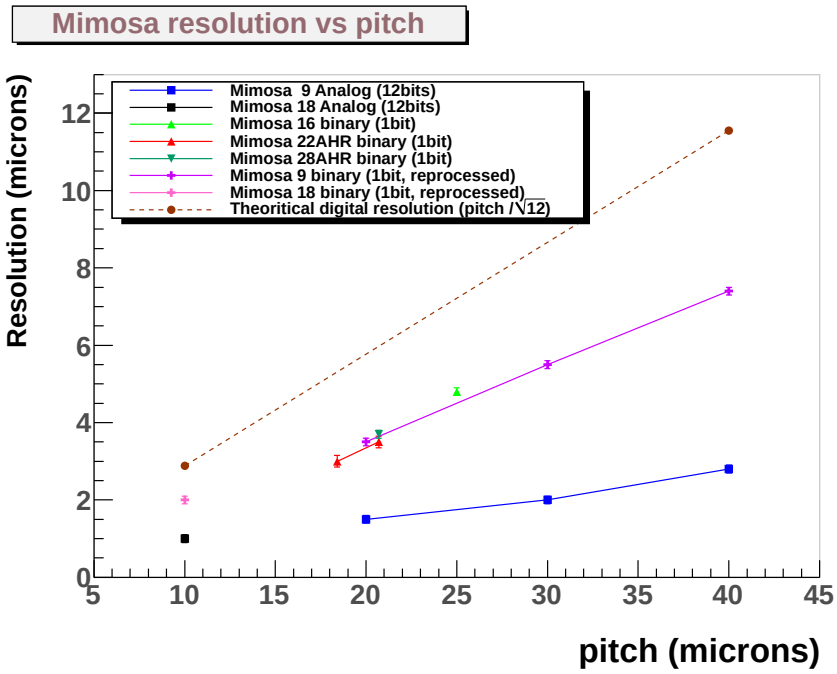

Figure 13: Resolutions of various CMOS sensors with analog or digital output, measured in test beam in function of the pixel pitch.

made from different segments inside the epitaxial layer with possible different x and y positions, one can expect a significant evolution in the model distributions when the angle is increased.

The plots of the figure 17 shows a comparison of the multiplicity distributions between test beam data of the Ultimate sensor for different discriminator thresholds and different incident angles. The bin by bin difference is also shown on figure 18. The agreement remains satisfactory within $\simeq 10 - 15\%$. Thus the model can be safely used with any incident angle as long as it is not too large (below 60 deg.).

References

[1] R. Turchetta *et al.*, *A Monolithic Active Pixel Sensor for Charged Particle Tracking and Imaging Using Standard VLSI CMOS Technology*, Nucl.Instr.Meth. in Phys. Res. A458 (2001) 677-689.

[2] G. Voutsinas *et al.*, *Studies for a 10μs, thin, high resolution CMOS pixel sensor for future vertex detectors*, Nucl. Phys. B - Proc. Suppl. 215 (2011) 48-50, and references therein. Nucl.Instr.Meth. A650 (2011) 208-212. see also *http://www.iphc.cnrs.fr/PLUME.html*.

[3] A. Besson, *DIGMAPS: a digitizer tool for MAPS*. Available here *http://www.iphc.cnrs.fr/Public-documentation.html*

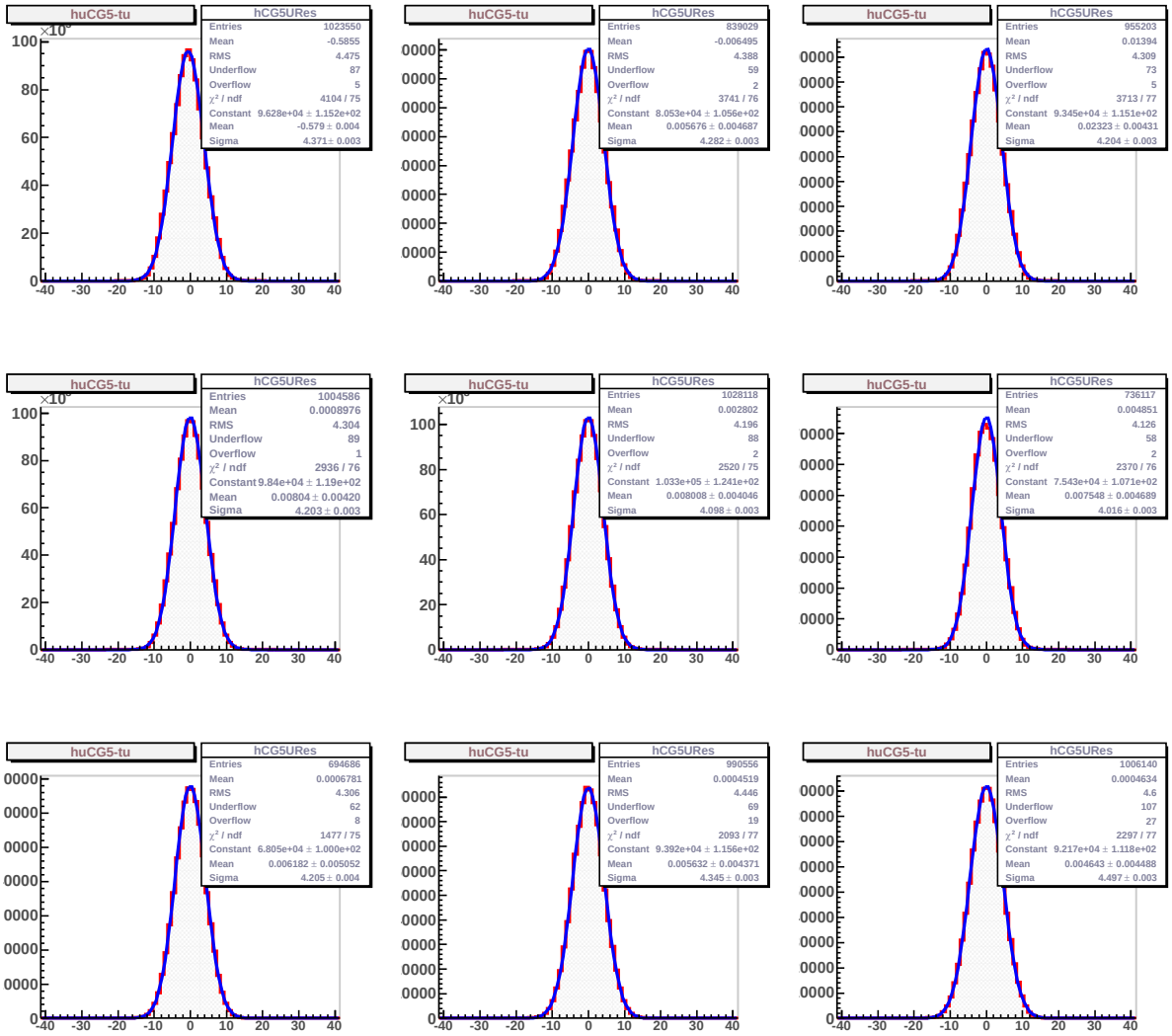

Figure 14: For 9 different discriminator thresholds (from up left to bottom right, S/N $\geq$ 4.0, 4.5, 5.0, 5.8, 7.0, 8.0, 9.0, 10.2, 11.5), resolution with a center of gravity obtained with the digitiser model (effective epitaxial layer thickness = 9 μm).

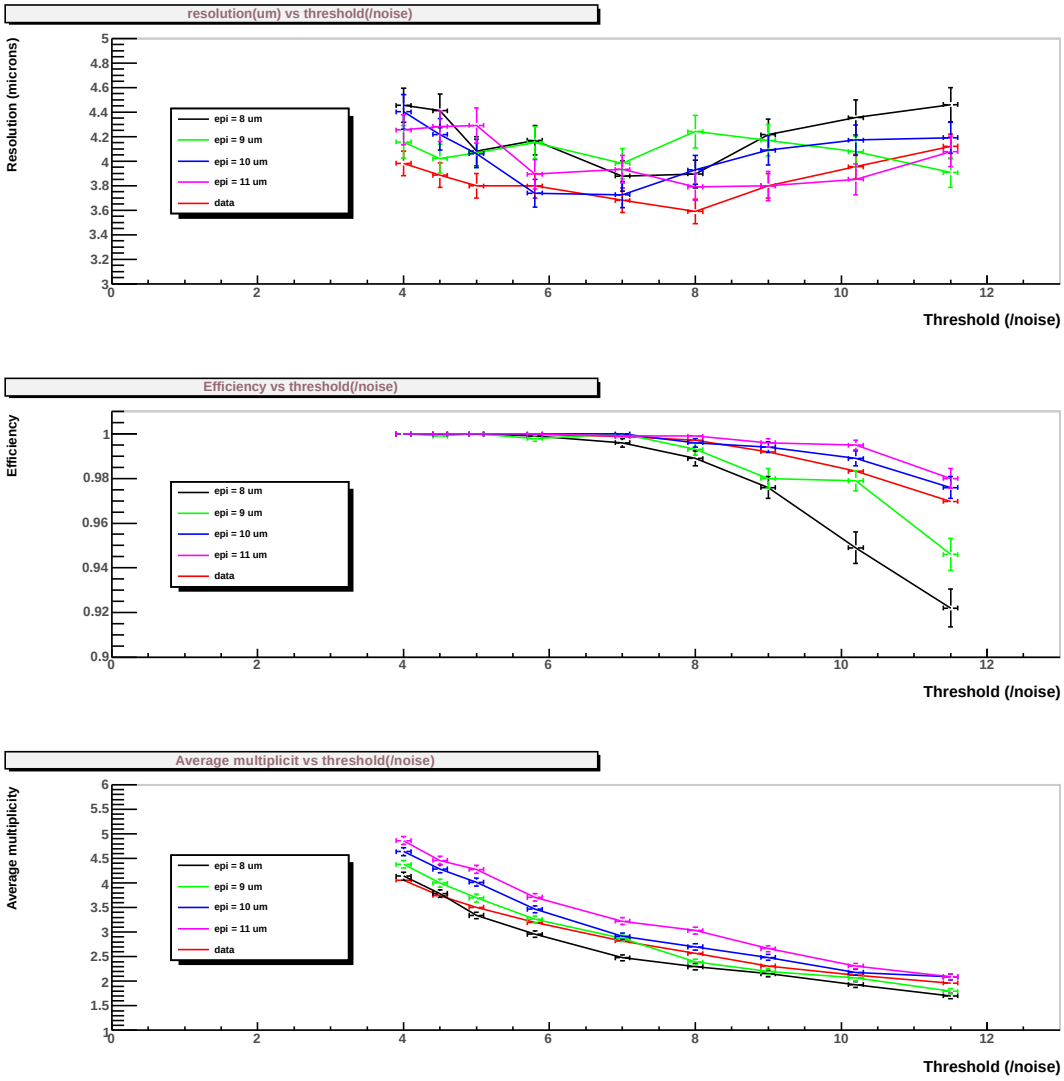

Figure 15: Top: resolution versus discriminator threshold (/noise)
Middle: Efficiency versus discriminator threshold (/noise)
Bottom: Average cluster multiplicity versus discriminator threshold (/noise)
a. red line filled in brown represents ultimate test beam data.
b. The four other colors represent the digitiser model with 4 different effective epitaxial layer thickness: black = 8 μm, green = 9 μm, blue = 10 μm, pink = 11 μm.

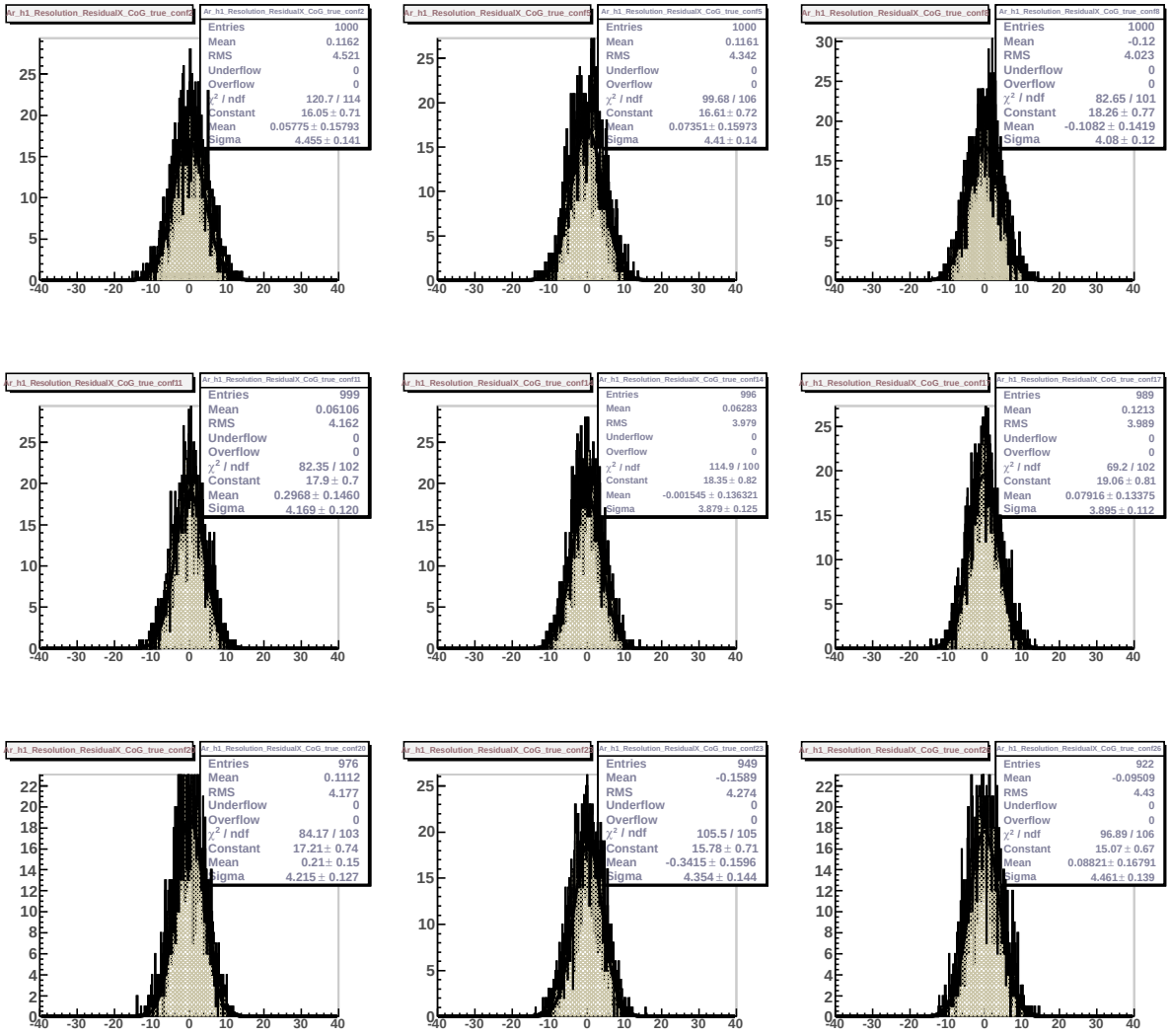

Figure 16: ultimate test beam data **Residual** for different thresholds. (from up left to bottom right, S/N $\geq$ 4.0, 4.5, 5.0, 5.8, 7.0, 8.0, 9.0, 10.2, 11.5). the ultimate resolution is obtained with: $\sigma_{data} = \sqrt{\sigma^2_{residual} - \sigma^2_{telescope}}$ with $\sigma_{telescope} = 1.8\mu m$.

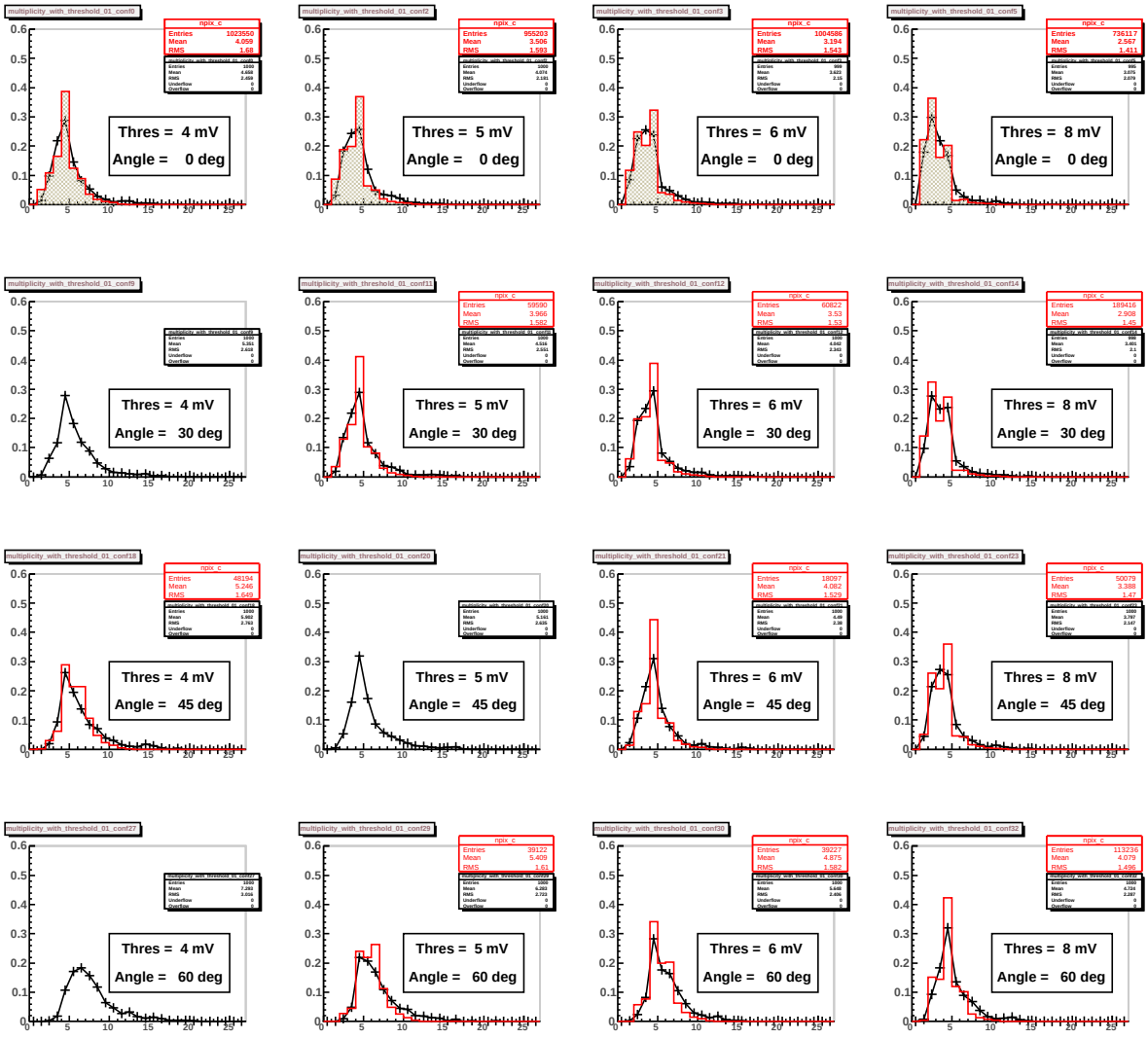

Figure 17: Cluster Multiplicity distribution for 4 different discriminator thresholds and 4 different incident particle angle (from up left to right, S/N $\geq$ 4.0, 5.8, 8.0, from top to bottom, Angle $= 0,\ 30,\ 45,\ 60$ deg.). a. red line filled in brown represents ultimate test beam data. b. The black line represents the digitiser model (effective epitaxial layer thickness = 9 μm)..

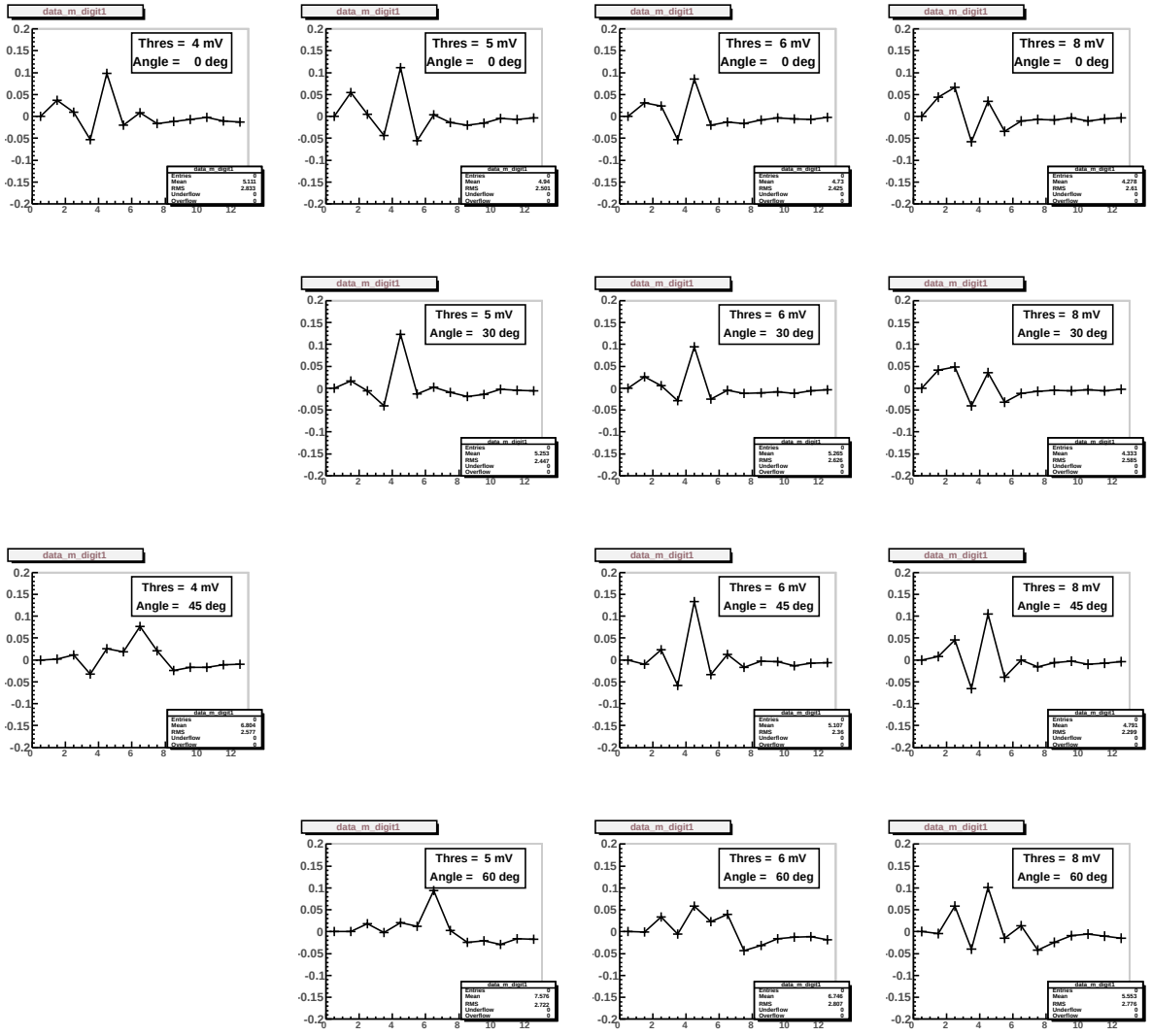

Figure 18: Cluster Multiplicity bin by bin difference between data and simulation model (effective epitaxial layer thickness = $9\ \mu m$). (from up left to right, S/N $\geq$ 4.0, 5.8, 8.0, from top to bottom, Angle $= 0,\ 30,\ 45,\ 60$ deg.).